Thermochimica Acta 477 (2008) 32–37

Contents lists available at ScienceDirect

Thermochimica Acta

journal homepage: www.elsevier.com/locate/tca

Thermal conductivity measurement of anisotropic material using photothermal deflection method

P.S. Jeon [a], J.H. Kim [a], H.J. Kim [b,*], J. Yoo [b]

[a] Department of Mechanical Engineering, Ajou University, Wonchun-dong, Yeongtong-gu, Suwon 443-749, Republic of Korea
[b] Division of Mechanical Engineering, Ajou University, Wonchun-dong, Yeongtong-gu, Suwon 443-749, Republic of Korea

ARTICLE INFO

Article history:
Received 14 November 2007
Received in revised form 2 May 2008
Accepted 6 August 2008
Available online 22 August 2008

Keywords:
Thermal conductivity
Anisotropic material
Photothermal deflection method

ABSTRACT

A complete theoretical treatment of photothermal deflection spectroscopy has been performed for the measurement of thermal conductivities in an anisotropic medium. An analytical solution of three-dimensional heat conduction was obtained by using 2D Fourier Transforms for an anisotropic material irradiated by a laser beam. Thermal conductivity was determined by using the phase angle of deflection at relative positions between the heating and probe beams. Excellent agreement between theoretical and experimental photothermal deflections was obtained. Also, the thermal conductivity in an arbitrary measurement direction for anisotropic materials (Pyrolytic graphite) was measured.

1. Introduction

Photoacoustic and photothermal techniques have received much interest in their use for the determination the structural, thermal, and optical properties of materials. Thermal properties of materials have been studied by various methods such as photothermal radiometry, photothermal refraction, photothermal deflection, and photothermal displacement. In this study, we adopted the photothermal deflection method, which is called the probe-beam-deflection method (mirage). This method requires no mechanical contact with the specimen, and thus thermal properties can be measured without the limit of sample size. It was introduced by Jackson et al. [1] and has since then proved to be a useful tool in the study of optical and thermal properties of isotropic materials. Also, it has been applied in fields of nondestructive evaluations and photothermal imaging.

This method is based on the heating of the specimen by a modulated beam (light source). The light source is converted into heat energy, which induces thermoelastic waves within the sample. The heat flow on the sample surface produces a refractive index gradient in the adjacent medium. A second laser beam (probe beam) is injected in parallel with the heated surface so that the beam can be deflected by the mirage effect. The analysis of this deflection leads to the determination of the thermal properties of the sample. The three-dimensional deflection has been extensively reported in previous research on isotropic media [1–5], but only a few papers have dealt with anisotropic materials. Therefore, measurement techniques for anisotropic materials, as well as their accurate measurement of thermal properties, are necessary. Moreover, directional thermal property should be measured.

A three-dimensional heat conduction equation was derived to describe the thermal wave propagation in anisotropic media by Iravani and Nikoonahad [6]. And mirage and radiometry method for a principal conductivity system was studied by Salazar et al. [7].

In this study, we have obtained the solutions of a three-dimensional thermal conduction equation for anisotropic materials by using nonsymmetric-Fourier transforms. A comprehensive theoretical analysis has been carried out on the photothermal deflection method in the measurement of thermal conductivities for anisotropic materials. Also, the modulation frequency of the heating beam, the thermal conductivity, and the angle between crystalline direction and experiment direction was studied by parametric study. As an application, the thermal conductivity in an arbitrary direction of an anisotropic material (Pyrolytic graphite) was measured through the matching process between theoretical and experimental results.

2. Theory and principle

We assume that the heating beam propagates through the sample in the z direction, centered at the origin of the coordinate system, as shown in Fig. 1. The probe beam deflection angle is

* Corresponding author. Tel.: +82 31 219 2340; fax: +82 31 213 7108.
E-mail address: hyunkim@ajou.ac.kr (H.J. Kim).

0040-6031/$ – see front matter © 2008 Elsevier B.V. All rights reserved.
doi:10.1016/j.tca.2008.08.004

Nomenclature

a	radius of the pump beam (m)
f	modulation frequency (Hz)
k	thermal conductivity (W/m K)
l	thickness of sample (m)
n	reflective index
P	absorption energy (W)
Q	heat source (W/m^3)
q	heat flux (W/m^2)
q_x, q_y	integration parameter
T	temperature (K)
t	time (s)

Greek letters

α	thermal diffusivity (m^2/s)
φ	deflection angle (°)
λ	optical absorption coefficient (m^{-1})
ω	angular frequency (s^{-1})

represented by the well-known formula [1].

$$\varphi = -\left(\frac{1}{n}\right)\left(\frac{\mathrm{d}n}{\mathrm{d}T}\right)\int_s \nabla_t T\,\mathrm{d}s \tag{1}$$

where n, T and ∇_t denote, respectively, the refractive index, the temperature rise, and the gradient transverse to the probe beam paths. In order to solve Eq. (1), analysis of the temperature distributions of the sample and the atmosphere at its periphery should be carried out. Then, the obtained temperature distribution equation is then inserted into the Eq. (1), and the final deflection phase angle of the probe beam can be obtained.

2.1. Temperature distribution

To obtain an expression for the photothermal deflection, we consider a homogeneous and anisotropic infinite plate of finite thickness (l) with stress-free boundaries, which is irradiated by a sinusoidally modulated laser beam of power that is incident normally to the sample surface [6,8,9].

The temperature distribution within the anisotropic sample is given by the solution of the following generalized 3D conduction equation:

$$\nabla\cdot\{\vec{k}\times\nabla T_i\} - \rho c\frac{\partial T_i}{\partial t} = Q_i \quad (i = \mathrm{g, m, r}) \tag{2}$$

where $T(x,y,z,t)$ is the temperature in the sample, k is the thermal conductivity tensor, ρ is density, c is specific heat, and $Q(x,y,z,t)$ is the power per unit volume deposited by the heating beam. And the subscripts g, r indicate the front and rear gases of the specimen and the subscript m represents the domain of the specimen.

The temperature and heat flux continuity conditions are

$$\begin{aligned} T_\mathrm{g}(x,y,0) &= T_\mathrm{m}(x,y,0), \qquad q_\mathrm{g}(x,y,0) = q_\mathrm{m}(x,y,0),\\ T_\mathrm{m}(x,y,l) &= T_\mathrm{r}(x,y,l), \qquad q_\mathrm{m}(x,y,l) = q_\mathrm{r}(x,y,l), \end{aligned} \tag{3}$$

where

$$q_\mathrm{m} = -\left(k_{31}\frac{\partial T_\mathrm{m}}{\partial x} + k_{32}\frac{\partial T_\mathrm{m}}{\partial y} + k_{33}\frac{\partial T_\mathrm{m}}{\partial z}\right),$$

$$q_i = -k_i\frac{\partial T_i}{\partial z} \quad (i = \mathrm{g, r}).$$

Also, because the temperature of the specimen by the heating beam rises very little, the heat transfer by convection or radiation can be considered negligible.

The heat source would be the laser beam characterized by a Gaussian intensity distribution and modulated with frequency (f). The beam radius (a) is defined at the $1/e$ of the intensity and the absorption coefficient (λ) is defined using the exponential law of light absorption. At the front and rear gas regions, light energy is not absorbed; therefore, the heat source is given by

$$Q_\mathrm{m}(x,y,z,t) = -\left(\frac{P}{4\pi a^2}\right)\mathrm{e}^{-\lambda z}\mathrm{e}^{-(x^2+y^2)/a^2}\mathrm{e}^{\mathrm{i}\omega t} \tag{4}$$

where the P represents the absorbed energy into the specimen and is decided by the output power of the heating beam and the reflectivity of the specimen. The heat source $Q(x,y,z,t)$ consists of a time-independent term and a term that always oscillates with a constant modulation frequency. The time-independent term is not considered since it does not have an effect on the phase of the deflection and thus only the time-dependent term is considered. The analysis of the heat conduction equation is simplified by the transformation of a periodic function of time into a steady state function. And to obtain the phase difference of the deflection angle, the heat conduction equation, Eq. (2) is transformed into Eq. (5) by applying a complex method, as follows

$$\begin{aligned} &k_{11}\frac{\partial^2\tilde{T}_\mathrm{m}}{\partial x^2} + k_{22}\frac{\partial^2\tilde{T}_\mathrm{m}}{\partial y^2} + k_{33}\frac{\partial^2\tilde{T}_\mathrm{m}}{\partial z^2} + (k_{12}+k_{21})\frac{\partial^2\tilde{T}_\mathrm{m}}{\partial x\partial y}\\ &+(k_{13}+k_{31})\frac{\partial^2\tilde{T}_\mathrm{m}}{\partial x\partial z} + (k_{23}+k_{32})\frac{\partial^2\tilde{T}_\mathrm{m}}{\partial y\partial z}\\ &= \mathrm{i}\omega\rho c\tilde{T} - \left(\frac{P\lambda}{4\pi a^2}\right)\mathrm{e}^{-\lambda z}\mathrm{e}^{-(x^2+y^2)/a^2} \end{aligned} \tag{5}$$

where

$$T_i(x,y,z,t) = \tilde{T}_i(x,y,z)\exp(\mathrm{i}\omega t)$$

Applying 2D Fourier transforms to Eq. (5), the equations are

$$\frac{\partial^2\tau}{\partial z^2} + \Gamma_1\frac{\partial\tau}{\partial z} + \Gamma_2\tau = \Gamma_3\,\mathrm{e}^{-\lambda z} \tag{6}$$

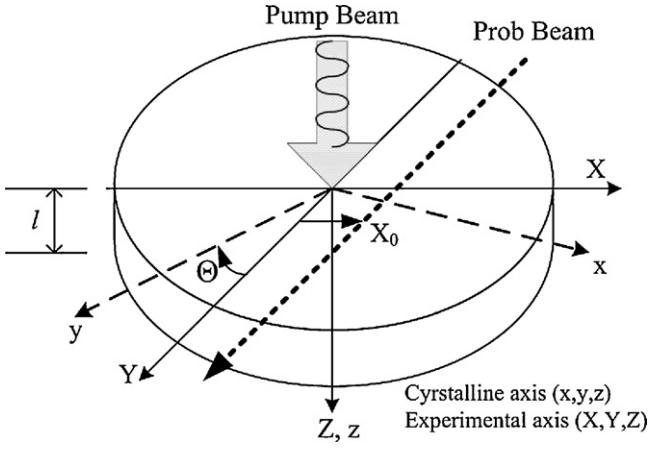

Fig. 1. Schematic description of the geometrical configuration: The probe beam has a transverse offset X_0 with respect to the pump beam.

where

$$\tau_i(q_x, q_y, z) = \left(\frac{1}{2\pi}\right)\int\int_{-\infty}^{\infty} \mathrm{e}^{\mathrm{i}(q_x x+q_y y)}\tilde{T}_i(x, y, z)\,\mathrm{d}x\,\mathrm{d}y$$

$$\Gamma_1 = \frac{-i\{(k_{13}+k_{31})q_x + (k_{23}+k_{32})q_x\}}{k_{33}}$$

$$\Gamma_2 = \frac{-\{k_{11}q_x^2 + k_{22}q_y^2 + (k_{12}+k_{21})q_x q_y + i\rho c\omega\}}{k_{33}}$$

$$\Gamma_3 = -\left(\frac{P\lambda/8\pi k_{33}}{\exp\{(q_x^2+q_y^2)a^2/4\}}\right).$$

The boundary conditions, which are transformed by the complex method and the 2D Fourier transforms, are

$$k_{\mathrm{g}}\left.\frac{\partial\tau_{\mathrm{g}}}{\partial z}\right|_{z=0} = -\mathrm{i}(k_{31}q_x + k_{32}q_y)\tau_{\mathrm{m}} + k_{33}\left.\frac{\partial T_{\mathrm{m}}}{\partial z}\right|_{z=0},$$

$$-\mathrm{i}(k_{31}q_x + k_{32}q_y)\tau_{\mathrm{m}} + k_{33}\left.\frac{\partial\tau_{\mathrm{m}}}{\partial z}\right|_{z=l} = k_{\mathrm{r}}\left.\frac{\partial\tau_{\mathrm{r}}}{\partial z}\right|_{z=l}, \quad (7)$$

$$\tau_{\mathrm{g}}|_{z=0} = \tau_{\mathrm{g}}|_{z=0}, \quad \tau_{\mathrm{m}}|_{z=l} = \tau_{\mathrm{r}}|_{z=l}.$$

Eq. (6) is the 2nd-order differential equation, and the solution to this equation is written as Eq. (8). In addition, coefficients A_1, A_2, B, and C are obtained from the transformed boundary conditions, Eq. (7).

$$\tau_{\mathrm{g}} = B\,\mathrm{e}^{m_{\mathrm{g}}z}, \quad \tau_{\mathrm{m}} = A_1\,\mathrm{e}^{m_1 z} + A_2\,\mathrm{e}^{m_2 z} + F\,\mathrm{e}^{-\lambda z}, \quad \tau_{\mathrm{r}} = C\,\mathrm{e}^{-m_{\mathrm{r}}z}, \quad (8)$$

where

$$F = \frac{\Gamma_3}{\lambda^2 - \lambda\Gamma_1 + \Gamma_2},$$

$$A_1 = \frac{(\xi+m_2+\gamma_{\mathrm{r}}m_{\mathrm{r}})(\xi-\lambda-\gamma_{\mathrm{g}}m_{\mathrm{g}})\mathrm{e}^{m_2 l} - (\xi+m_2-\gamma_{\mathrm{g}}m_{\mathrm{g}})(\xi-\lambda+\gamma_{\mathrm{r}}m_{\mathrm{r}})\mathrm{e}^{-\lambda l}}{(\xi+m_1+\gamma_{\mathrm{r}}m_{\mathrm{r}})(\xi+m_2-\gamma_{\mathrm{g}}m_{\mathrm{g}})\mathrm{e}^{m_1 l} - (\xi+m_1-\gamma_{\mathrm{g}}m_{\mathrm{g}})(\xi+m_2+\gamma_{\mathrm{r}}m_{\mathrm{r}})\mathrm{e}^{m_2 l}}F,$$

$$A_2 = \frac{(\xi+m_1-\gamma_{\mathrm{g}}m_{\mathrm{g}})(\xi-\lambda+\gamma_{\mathrm{r}}m_{\mathrm{r}})\mathrm{e}^{-\lambda l} - (\xi+m_1+\gamma_{\mathrm{r}}m_{\mathrm{r}})(\xi-\lambda-\gamma_{\mathrm{g}}m_{\mathrm{g}})\mathrm{e}^{m_1 l}}{(\xi+m_1+\gamma_{\mathrm{r}}m_{\mathrm{r}})(\xi+m_2-\gamma_{\mathrm{g}}m_{\mathrm{g}})\mathrm{e}^{m_1 l} - (\xi+m_1-\gamma_{\mathrm{g}}m_{\mathrm{g}})(\xi+m_2+\gamma_{\mathrm{r}}m_{\mathrm{r}})\mathrm{e}^{m_2 l}}F,$$

$$B = A_1 + A_2 + F, \quad C = A_1\,\mathrm{e}^{l(m_1+m_{\mathrm{r}})} + A_2\,\mathrm{e}^{l(m_2+m_{\mathrm{r}})} + F\,\mathrm{e}^{l(m_{\mathrm{r}}-\lambda)},$$

$$\xi = -\frac{i(k_{31}q_x + k_{32}q_y)}{k_{33}},$$

$$m_1 = \frac{-A_1 + \sqrt{A_1^2 - 4A_2}}{2}, \quad m_2 = \frac{-A_1 - \sqrt{A_1^2 - 4A_2}}{2},$$

$$m_i = \sqrt{\frac{q_x^2 + q_y^2 + \mathrm{i}\omega}{\alpha_i}} \quad (i = \mathrm{g}, \mathrm{r}).$$

Using Inverse Fourier Transforms and the complex method, the equations of the final temperature distribution are obtained as follows.

$$T_i(x, y, z, t) = \frac{\mathrm{e}^{\mathrm{i}\omega t}}{2\pi}\int\int_{-\infty}^{\infty}\mathrm{d}q_x\,\mathrm{d}q_y\,\tau(q_x, q_y, z) \quad (9)$$

2.2. Probe beam deflection

The rectangular coordinate is used to analyze the probe beam deflection, as shown in Fig. 1(a). The deflection of the probe beam having a vector structureis comprised of the lateral (φ_{l}) and the normal (φ_{n}) component. In this study, the lateral direction corresponds to the Y-direction coordinate and the normal direction to the Z-direction. The refractive index and the thermal coefficient index are atmospheric values because the probe beam passes through air above the surface of the specimen. The deflection angles can be formulated for the lateral direction and normal direction, as shown as Eq. (10), including the temperature variable (T_{g}) in the integral term [1].

$$\varphi_{\mathrm{l}} = -\left(\frac{1}{2\pi n}\right)\left(\frac{\mathrm{d}n}{\mathrm{d}T}\right)_{\mathrm{g}}\int_s\frac{\partial T_{\mathrm{g}}}{\partial X}\,\mathrm{d}Y, \quad \varphi_{\mathrm{n}} = -\left(\frac{1}{n}\right)\left(\frac{\mathrm{d}n}{\mathrm{d}T}\right)_{\mathrm{g}}\int_s\frac{\partial T_{\mathrm{g}}}{\partial Z}\,\mathrm{d}Y \quad (10)$$

The two components of the probe beam deflection are obtained as follows.

$$\varphi_l = \left(\frac{1}{2\pi n}\right)\left(\frac{\mathrm{d}n}{\mathrm{d}T}\right)_{\mathrm{g}}\int\int\int_{-\infty}^{\infty}\mathrm{d}Y\,\mathrm{d}q_x\,\mathrm{d}q_y\,\mathrm{e}^{m_{\mathrm{g}}Z}B(q_x, q_y)$$
$$\times\mathrm{e}^{-\mathrm{i}X(q_x\cos\Theta - q_y\sin\Theta)}\cdot\mathrm{e}^{-\mathrm{i}Y(q_x\sin\Theta + q_y\cos\Theta)}\cdot\mathrm{i}(q_x\cos\Theta - q_y\sin\Theta)$$
$$\times\varphi_{\mathrm{n}} = -\left(\frac{1}{2\pi n}\right)\left(\frac{\mathrm{d}n}{\mathrm{d}T}\right)_{\mathrm{g}}\int\int\int_{-\infty}^{\infty}\mathrm{d}Y\,\mathrm{d}q_x\,\mathrm{d}q_y\,\mathrm{e}^{m_{\mathrm{g}}Z}B(q_x, q_y)$$
$$\times\mathrm{e}^{-\mathrm{i}X(q_x\cos\Theta - q_y\sin\Theta)}\cdot\mathrm{e}^{-\mathrm{i}Y(q_x\sin\Theta + q_y\cos\Theta)} \quad (11)$$

3. Experimental apparatus

Fig. 2 shows the experimental apparatus and the schematic optical alignment. The pump beam, as the heating source, is a continuous Ar-ion laser (Spectra-Physics 2210) of 488 nm wavelength and approximately 800 μm diameter, having a Gaussian intensity distribution. The pump beam is modulated as sine waves using an A/O modulator (A.A. Sa, AA.MT. 80/A 1.5) controlled by a lock-in amplifier (EG&G 5302). This modulated beam is controlled to make the diameter of the beam about 110–120 μm.

The probe beam is a He-Ne laser (Newport 1123P) of 633 nm wavelength and 5 mW power. A specimen is located at a position where it is normal to the pump beam, and fixed on the rotation stage with 1/60° resolution and on a linear stage with 0.5 μm resolution to satisfy the parallel condition to the probe beam. The deflection angle is detected by a photoelectric position sensor (Hamamatsu S2044). After signals from the position sensor go through the first amplifier, they are synchronized with a signal of the A/O modulator in a lock-in amplifier to obtain the phase difference between the two signals.

The thermal conductivities are measured by the detection of the phase difference between the pump beam and the probe beam at each relative position in 5–50 μm steps.

4. Results and discussion

4.1. Parametric study

The deflection and phase angle are generally used to determine the thermal property of a material in the photothermal deflection method. Here, the phase angle is defined as the phase lag between the deflected probe beam and the pump beam (undeflected probe beam). The deflection and phase angles are established through the numerical integration of various relative positions. The deflection angle of the probe beam at the front-air region is largely influenced by the modulation frequency (f), the thermal conductivity (k) and the angle between the crystallographic axis and the experimental axis. In addition, the refractive index, thermal expansion coefficient, and power of the heating beam in Eq. (11) affect the constants that increase or decrease the amplitude of deflection.

The thermal conductivity in region m is set as an orthorhombic system (k_{11} = 250 W/mK, k_{22} = 50 W/mK, k_{33} = 100 W/mK), and the atmosphere is set as the medium in regions g and r. The thickness of the sample is set as 1 μm; the radius of the heating beam as 100 μm; the absorbed energy as 0.25 W; the vertical distance between the probe beam and specimen as 20 μm; the modulation frequency as 200 Hz; and the angle between the experimental and the crystalline axis as 60°.

4.1.1. Temperature analysis

The variation of anisotropic properties such as the thermal conductivity can conveniently be illustrated by a “representation

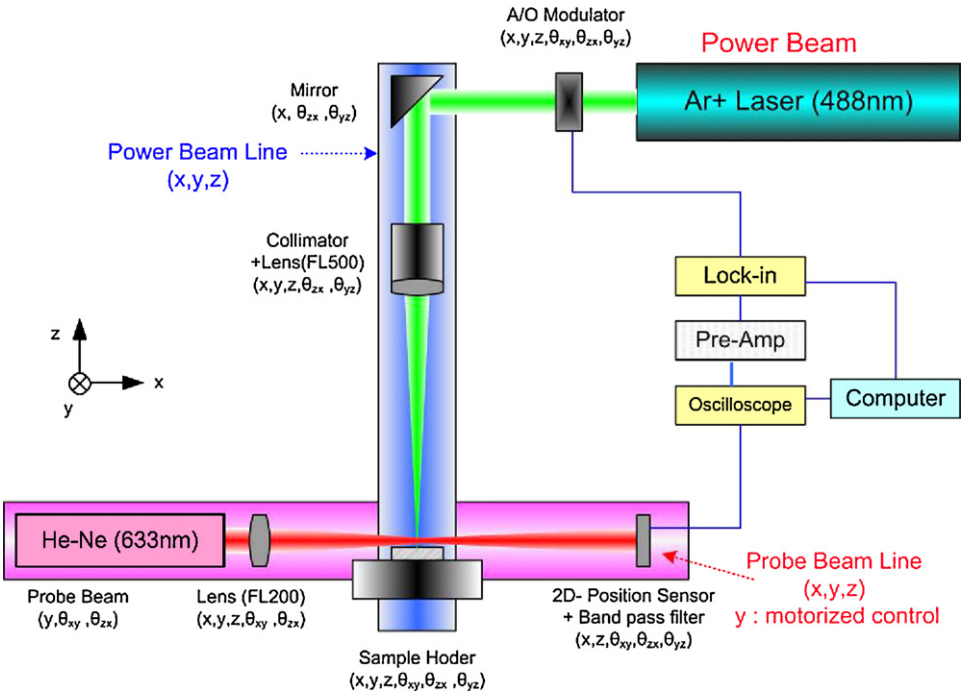

Fig. 2. Experimental apparatus and optical alignment for photothermal deflection method.

surface". In many cases, this is an ellipsoid, as shown in Fig. 3. The direction of heat flow in the orthorhombic anisotropic system is no longer parallel to that of the temperature gradient, except in the directions of the principal axes (which here, correspond to the semi-axes of the ellipse). The direction of the heat flux is always parallel to the normal to the tangential plane drawn at the point at which the direction of the temperature gradient intersects the representation ellipsoid; this is called the radius-normal property.

Suppose a three-dimensional temperature gradient, ∇T, lies along a direction specified by direction cosines l, m and n, where, for example, l is the cosine of the angle between the x-axis and the temperature gradient vector. Then, the components of the temperature gradient and heat flux parallel to the principal axes will be

$$\begin{aligned} &\nabla T_x = (\nabla T)l, \quad \nabla T_y = (\nabla T)m, \quad \nabla T_z = (\nabla T)n, \\ &q_x = k_{11}(\nabla T)l, \quad q_y = k_{22}(\nabla T)m, \quad q_z = k_{33}(\nabla T)n, \end{aligned} \tag{12}$$

where k_{xx}, k_{yy} and k_{zz} are the values of the thermal conductivity along the principal axes, x, y and z, and are called the principal values.

Hence, resolving back along the direction of the temperature gradient, the heat flux is

$$q_{\parallel} = q_x l + q_y m + q_z n = (k_{11}l^2 + k_{22}m^2 + k_{33}n^2)\nabla T = k_{\text{eff}}\nabla T. \tag{13}$$

Thus, the value of the thermal conductivity (effective thermal conductivity), k_{eff}, is defined as follows.

$$k_{\text{eff}} = k_{11}l^2 + k_{22}m^2 + k_{33}n^2 \tag{14}$$

where the directional cosines in our measurement condition are $\cos\Theta$, $\sin\Theta$ and 0, respectively.

The influence by the anisotropic ratio (k_{11}/k_{22}) on the temperature profile of the sample surface, $T(x,y,z=0)$ is investigated in Fig. 4. If $k_{11} = k_{22}$, the contour shape of the temperature profile is a circle, and the direction of heat flow is parallel to that of the temperature gradient. But if $k_{11} \neq k_{22}$, this section is an ellipse, and the direction of heat flow is no longer parallel to that of the temperature gradient, except in the directions of the principal axes (which here correspond to the semi-axes of the ellipse). Depending on the relative values of k_{11} and k_{22}, the contour shape of the temperature profile is either a rugby ball shape ($k_{11} < k_{22}$) or a Smartie shape ($k_{11} > k_{22}$).

Fig. 5 shows the typical plot of a temperature distribution at the surface obtained by using Eq. (9). There are some differences according to the analysis condition such as thermal diffusivity, thermal conductivity, thermal expansion coefficient, reflectivity, and optical absorption coefficient, but the range of the temperature difference is from 2 to 5 K usually. Because the temperature increment

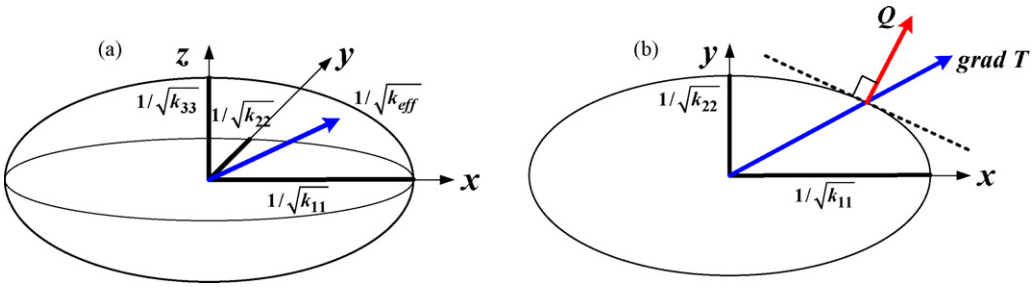

Fig. 3. Anisotropic thermal conductivity (anisotropic ellipsoid).

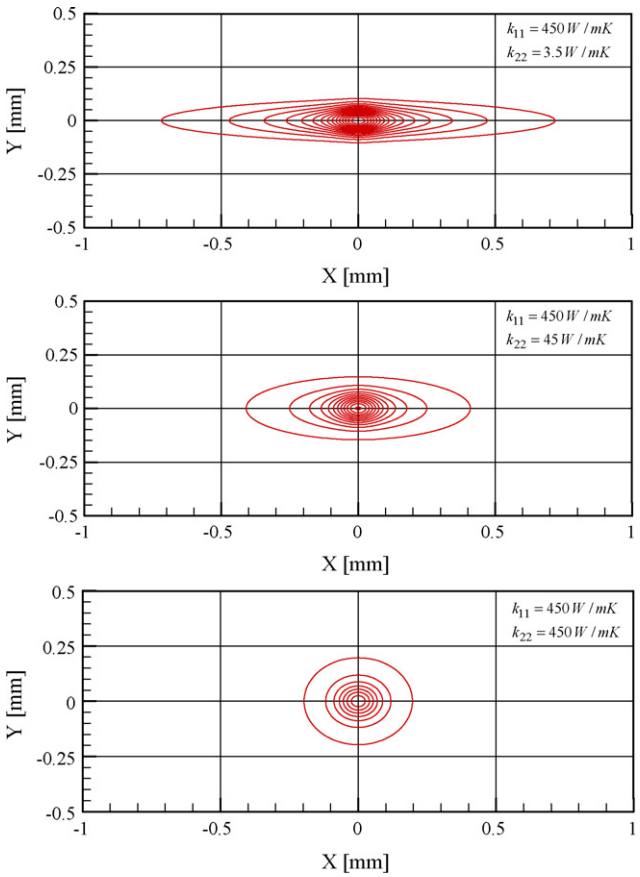

Fig. 4. Contours of constant magnitude of temperature field for different anisotropic ratios.

is very small, the measured value in this study could be considered the thermal conductivity of room temperature.

Because the thermal conductivity of materials is high, the maximum temperature becomes smaller, as shown in Fig. 3. These results are due to the fact that the absorbed energy in the material with high thermal conductivity diffuses faster than materials with relatively low thermal conductivity.

4.1.2. Probe beam deflection analysis

To optimize the experimental measurement conditions, the influences of parameters such as thermal conductivity, modulation frequency, and the angle between experimental and crystalline directions were analytically studied with respect to the phase angle.

The representative signals obtained by the photothermal deflection method are the amplitude and phase of the deflection angle. The measured signal in the normal direction is omitted because it is accompanied by many errors in analysis, which are the result of having more noises than the signal in the lateral direction. And the influences by modulation frequency and thermal conductivity on the phase angle have shown a similar result [10]. Modulated frequency and thermal conductivity are important parameters which affect the thermal diffusion length ($= \sqrt{k/\pi f \rho c}$). The decrease of the modulation frequency or the increase of the thermal conductivity means an increase of the thermal diffusion length. As the thermal diffusion length increases, the gradient of the phase of the lateral component also decreases. The temperature gradient on the surface decreases, and then, the amplitude of the probe beam deflection becomes small. Consequently, the value of the phase difference becomes small at the same relative position. Therefore, the measurable relative position becomes shorter.

Fig. 6 shows the calculated results for various angles (Θ) between the crystalline direction and the probe beam. As shown in Eq. (14), the changes of the angle are proportional to those of the effective thermal conductivity (k_{eff}). The influence of the effective thermal conductivity (k_{eff}) in anisotropic materials is similar to the effect of the thermal conductivity in isotropic materials. Therefore, if the effective thermal conductivity in the measurement surfaces of the samples is the same, the photothermal signal will be identical.

4.2. Experimental results

In the present study, iron and copper of 99.9% purity were used as isotropic materials to verify the theoretical results and the experimental apparatus shown in Fig. 2. The thermal conductivity values of iron and copper measured from experiments were 82.0 and 39.0 W/mK, respectively, and they were measured with accuracy of less than 2.1% error as compare them with the literature values [11].

The PG (Pyrolytic graphite) as anisotropic material, which is widely used for commercial objects, was chosen for experimental specimens. Fig. 6 shows the measured results of the phase angle at various probe beam angles. The thermal conductivity ranges between 3 and 420 W/mK. The experiments were performed at room temperature (20 °C) and hence, properties such as density and specific heat corresponded to the values at room temperature.

Fig. 7 shows the experimental results which were obtained at the same modulation frequency (f = 200 Hz) to determine explicitly

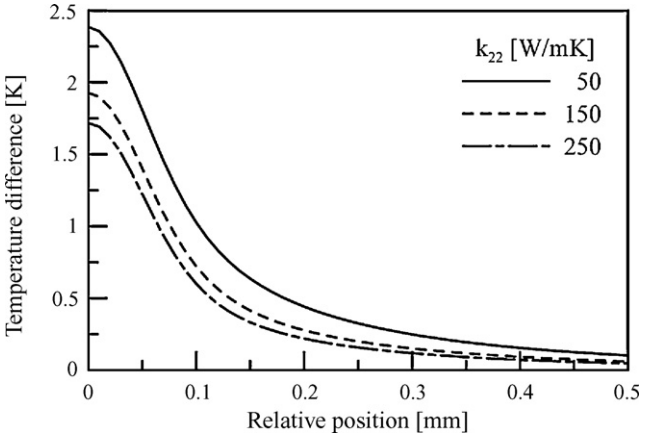

Fig. 5. Temperature distribution for various thermal conductivities (fixed k_{11} and k_{33}).

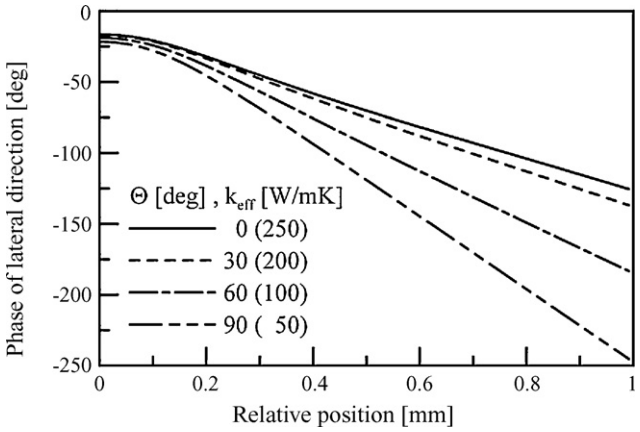

Fig. 6. Influence of each parameter Θ on the phase curve.

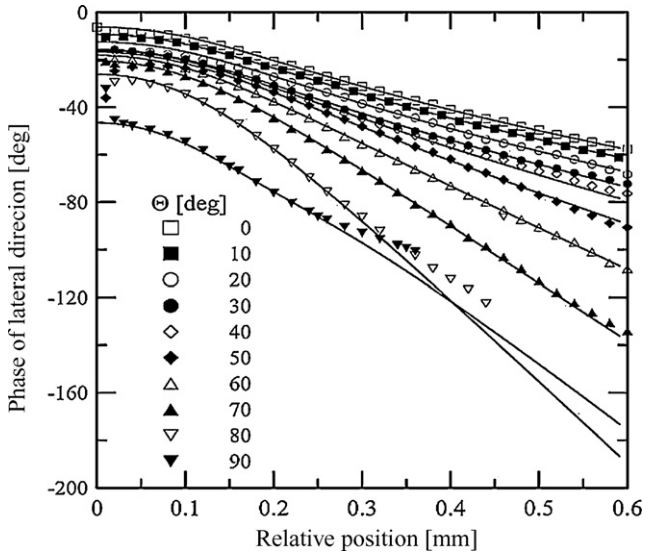

Fig. 7. Experimental results for various angles (Θ) between the crystallographic axis and the probe beam (phase of lateral direction).

how the effective thermal conductivity changes with the variations of the angle between the crystalline direction and the probe beam (experimental direction). In the cases of 80° and 90°, the measured data showed a large deviation from the theoretical results after the 0.3 mm relative position because the thermal diffusion length of the specimen was less than that of the adjacent gas (air). Consequently, the measured values in these areas had larger uncertainty than those in the other areas.

The photothermal signal versus the relative position between the pump and the probe beam along the sample is quite sensitive to the changes in the thermal properties of the sample. The region where the measured and theoretical phase curves agree well extends from one quarter to three quarters of the minimum position. An effective thermal conductivity is determined by a bi-section method when the standard deviation between the experimental and theoretical phase curve is minimized (The phase curve is the same when the value of k_{eff} is the same, even if the values of k_{11} and k_{22} are different, as shown in the Eq. (14)). But if the value of Θ is 0 or 90, the value of k_{eff} can be obtained easily, because one of the values of k_{11} and k_{22} will be zero. Also, the more measurements for the various Θ, the more reliable the k_{11} and k_{22} will become. And

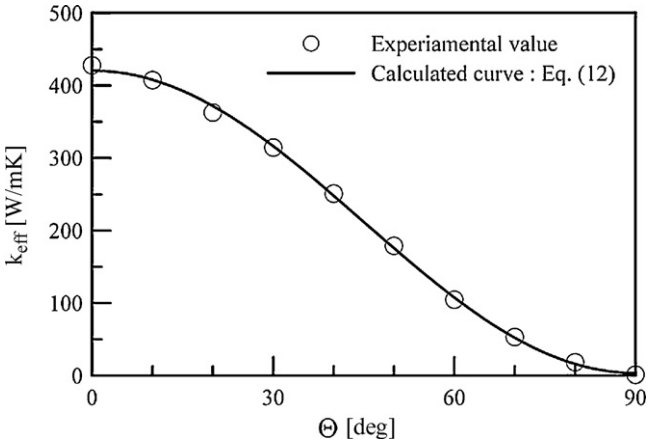

Fig. 8. Measured thermal conductivity as the function of angle (Θ) between the crystallographic axis and the probe beam.

the uncertainty of the photothermal deflection method is 1.4%. The major parameters are the radius of pump beam, vertical offset (relative distance between probe beam and sample surface) and sample thickness.

Fig. 8 shows the effective thermal conductivities obtained from Fig. 7 for various angles Θ. The solid line is calculated by fitting the experimental values with Eq. (12), which is used to determine the coefficients k_{11} and k_{22} of Eq. (12). The coefficient of determination (R-squared) between the measured thermal conductivities and the fitted curve in the whole range is 0.999241.

The thermal conductivities measured from this study are 420.5 W/mK for k_{11} and 3.5 W/mK for k_{22}, and these results are in the range of the literature values, from 240 to 1950 W/mK for k_{11} and from 1.7 to 5.7 W/mk for k_{22} [7,12–14].

5. Conclusion

In this study, we obtained the solutions of the three-dimensional thermal conduction equation for anisotropic materials using nonsymmetric-Fourier transforms. The influences of the parameters, such as the modulation frequency of the heating beam, the thermal conductivity tensor, and the angle between the experimental and crystallographic axes, were investigated. When the thermal conductivity of materials was high or the modulation frequency was low, the maximum value of the temperature decreased, and the gradient of the deflection phase curve also decreased. Furthermore, the changes of the measurement angle in anisotropic materials (the angle between a crystalline direction and probe beam) result in the differences of the effective thermal conductivity.

The experimental configuration based on the theoretical analysis was verified to identify the thermal conductivities of isotropic pure metals, and achieves the precise measurement within 2.1% error. The thermal conductivities for the commercial PG along crystalline directions were 420.5 W/mK for k_{11} and 3.5 W/mK for k_{22}. Also, thermal conductivity was measured for various measurement directions (the angle between the crystalline directions of the specimens and the probe beam).

Acknowledgements

This work was supported by Grant no. R01-2006-000-11264-0(2006) from the Basic Research Program of the Korea Science & Engineering Foundation and the Grant of Korea Science Engineering Foundation (R05-2004-000-11406).

References

[1] W.B. Jackson, N.M. Amer, A.C. Boccara, D. Fournier, Appl. Opt. 20 (1981) 1333–1344.
[2] D.L. Balageas, D.M. Boscher, A.A. Deon, F. Enguehard, ETPC Proc. 23 (1991) 517–528.
[3] A. Salazar, A. Sanchez-Lavega, J. Fernandez, J. Appl. Phys. 69 (1991) 1216–1223.
[4] B. Li, Z. Zhen, S. He, Appl. Phys. D 24 (1991) 2196–2201.
[5] M. Bertolotti, R. Li Voti, G. Liakhou, C. Sibilia, Rev. Sci. Instrum. 64 (1993) 1576–1583.
[6] M.V. Iravani, M. Nikoonahad, J. Appl. Phys. 62 (1987) 4065–4071.
[7] A. Salazar, A. Sanchez-Lavega, A. Ocariz, Appl. Phys. Lett. 67 (1995) 626–628.
[8] P.S. Jeon, K.J. Lee, J. Yoo, Y.M. Park, J.H. Lee, KSME Int. J. 17 (2003) 2078–2086.
[9] H.S. Carslaw, J.C. Jaeger, Conduction of Heat in Solids, Oxford University Press, 1959.
[10] K.J. Lee, J.O. Kang, P.S. Jeon, B.N. Jo, J. Yoo, H.J. Kim, J. Kor. Phys. Soc. 51 (2007) S36–S41.
[11] American Institute of Physics Handbooks, third ed., McGraw Hill, New York, 1982.
[12] GE Advanced Ceramics (http://www.advceramics.com).
[13] F.P. Incropera, D.P. Dewitt, Fundamentals of Heat and Mass Transfer, sixth ed., 2005.
[14] SPI Supplies® Brand Pyrolytic Graphite Planchets (http://www.2spi.com/catalog /mounts/pyrolytic-information.html).